A push in the right direction: exploring the role of Zealandia collision in Eocene Pacific-Australia plate motion changes

Dan Sandiford[1], Peter Betts[1], Joanne Whittaker[2], Louis Moresi[3]

[1]Monash University
[2]University of Tasmania, Institute of Marine and Antarctic Studies
[3]Australian National University

Key Points:

- During the Eocene tectonic reorganization, the Pacific Plate rotation vector developed an increased radial component (spin around the centroid) with a counter clockwise (CCW) sense
- Both the Zealandia plate boundary, and the Izu-Bonin-Marianas (IBM) margin, could efficiently partition plate boundary normal forces into CCW Pacific Plate radial torques at 47 Ma
- Recent numerical mantle convection simulations support our geometric analysis, particularly in terms of the role of the IBM

Corresponding author: Dan Sandiford, dansandifordscience@gmail.com

Abstract

The Pacific Plate underwent a significant change in motion during the early Eocene. The motion change has been linked to plate boundary reconfiguration, particularly in relation to the evolution of its subduction margins. The reconfiguration also resulted in a new Pacific-Australian plate boundary section transecting the rifted Gondwanan fragment of Zealandia. In the period ca. 47-32 Ma, the relative rotation axis of the Pacific and Australian Plates was located close to (often within) continental Zealandia. Previous studies have speculated that the Zealandia continental boundary could have acted as a pivot point for Pacific-Australia relative motion. Here we investigate the extent to which collision resistance along the intra-continental Zealandia boundary ($\sim$ 1000 km) might have impacted the motion of the Pacific Plate, which is characterised by trench and ridge lengths more than one order of magnitude higher. We first highlight a significant change in the radial component of the absolute Pacific Plate rotation at 47 Ma (i.e. the spin around the plate centroid axis) which helps to facilitate the relative pivoting between the Pacific and Australia. We then consider how parameterised plate boundary forces impact the tangential and radial components of the net torque vector (which includes both fictitious and true torque components). We show that during the Eocene transition, both the Zealandia boundary and the IBM subduction zone were well-oriented in terms of partitioning boundary-normal forces into CCW radial torques. The radial torque components were complimentary, while the tangential components were opposed, i.e. the two boundaries operate in the sense of a double-couple. The analysis predicts that the IBM should have had an anomalous influence on the radial component of Pacific torque, relative to the rest of the paleo-subduction margin at 47 Ma. This is supported by results from recent global scale numerical mantle convection simulations. The role of Zealandia cannot be established unambiguously, based on our analysis, but effects can be quantified under different assumptions. For instance, if collision resistance along the Zealandia boundary was comparable to the subduction force density at the IBM, the ratio of radial torque components is about 1/3. Zealandia could plausibly constitute a 'first order' effect, albeit only on the radial component of Pacific rotation, and probably subordinate to the role of the IBM. Overall the study suggests that the onset of Pacific-Australia pivoting at 47 Ma was a consequence of broader changes in the plate driving/resisting forces, as was unlikely to have been dominated by collision resistance across Zealandia.

1 Overview

This section covers two main issues: Firstly, we discuss the context and analytical approach of the paper, with particular emphasis on the dynamics of the Pacific Plate in the Cenozoic. Secondly, we briefly summarise the tectonic evolution of Zealandia, including the proposed role of the Hikurangi Plateau, from the middle Cretaceous. The section ends with an outline of the remainder of the paper.

1.1 Approach and context of study

This study is fundamentally motivated by questions relating to the relative motion of the Pacific and Australian plates during and following the major Eocene tectonic reorganisation (Whittaker et al., 2007). During the period ca. 47-32 Ma, the Euler Pole of Pac-Aus relative motion lay close to or within Zealandia (Sutherland, 1995; Keller, 2005). Reyners (2013) has suggested that collision resistance - involving the underthrust Hikurangi Plateau - may have had a 'first order' effect on plate motions.

In exploring this problem we will first highlight the fact that the absolute motion change of the Pacific Plate (ca. 47 Ma) comprises significant changes in both the tangential and radial components of the rotation vector. Both of these components have the effect of drawing the Euler Pole (of Pacific Plate absolute motion) towards Zealandia, as compared to the Pole locations prior to 47 Ma. Therefore Pacific Plate absolute motion appears to strongly facilitate the anchoring of relative (Aus-Pac) Euler Poles within or close to Zealandia at the same period.

Next we will analyse how different plate boundary normal forces contribute to the torque components that may drive such changes. The Zealandia boundary is shown to have a particularly high radial torque component, relative to tangential component, and the sign is consistent with the radial rotation change of the Pacific Plate (CCW). Furthermore, collision resistance forces are expected to evolve rapidly, in comparison to mantle buoyancy, and could therefore help to explain the rapidity of the Pacific motion change (Anderson, 2002; Hu et al., 2022). Based on these connections, our investigation, which begins with the effect of Zealandia on relative (Aus-Pac) motion, will ultimately focus on the capacity of Zealandia to effect the radial component of Pacific Plate torque - a subtle change in emphasis that we want to signal at the outset.

However, we cannot investigate the influence of the Zealandia plate boundary in isolation, particularly considering the long-standing concept that Eocene Pacific Plate motion changes can be dominantly attributed to the evolution of the subduction margins, including ridge subduction, cessation, initiation and polarity reversal (Whittaker et al., 2007; Wessel & Kroenke, 2008; Faccenna et al., 2012; Sutherland et al., 2017; Hu et al., 2022). The following paragraphs provide a brief background to these issues.

The evolution of Pacific Plate motion in the Cenozoic is connected with several important question in geodynamics, for instance: the role of subduction-related buoyancy distribution relative to other plate driving/resisting forces; the nature of the coupling between slabs and trailing plates; the causes of rapid changes in plate motion - particularly the Eocene change at around 47 Ma (Whittaker et al., 2007; Wessel & Kroenke, 2008; Faccenna et al., 2012; Hu et al., 2022).

Global plate motions are thought to be strongly influenced by the subduction-related buoyancy structure of the mantle (McKenzie, 1969; Hager & O'Connell, 1981; Becker & O'Connell, 2001; Conrad & Lithgow-Bertelloni, 2002; Ghosh & Holt, 2012). However, there remains significant debate regarding how the buoyancy structure related to past subduction is coupled to the surface plates. Some studies have advocated a strongly asymmetric coupling model, where a significant component of upper mantle slab buoyancy is directly coupled to the trailing plate (Elsasser, 1969; Conrad & Lithgow-Bertelloni, 2002). The magnitude of the resulting 'net slab pull' would constitute the dominant force acting on subducting plates, with expected force density magnitudes of $\mathcal{O}(10)$ TN/m. Other constraints, such as trends in the intra-plate stress field , geoid patterns over subduction zones, and predictions from dynamic subduction modelling, suggest the typical magnitude of the slab stress guide must be much lower than upper-end inferences (e.g., Conrad & Lithgow-Bertelloni, 2002). Such studies tend to predict that net slab pull should be on the same order as contributions from typical oceanic gravitation potential energy (GPE) variation ($\mathcal{O}(3)$ TN/m) (Hager & O'Connell, 1981; Moresi & Gurnis, 1996; Schellart, 2004; Sandiford et al., 2005; Coblentz et al., 2015). These lower-end estimates of net-slab pull may reflect strong flow-induced support of the slab in the mantle, mechanical weakness of the subducted lithosphere, or a combination of these factors (e.g., Forsyth & Uyeda, 1975; Hager & O'Connell, 1981; Moresi & Gurnis, 1996).

The primary analysis undertaken in this paper is to quantify the evolution of what Becker and O'Connell (2001) refer to as "parameterised plate boundary forces". In particular, we focus on the relative effects of collision resistance at Zealandia, compared with subduction related forces acting on the Pacific Plate margins. Similar approaches have previously been used to link changes in Pacific Plate motion to the evolution of slab pull forces (Faccenna et al., 2012; Iaffaldano & Lambeck, 2014), but also to suggest limitations of slab pull, at least in the absence of additional active mantle driving forces (Stotz et al., 2018; Rowley & Forte, 2022). In this study we do not consider the age of the lithosphere in estimating subduction-related forces, and hence the analysis is purely geometric (e.g., Iaffaldano & Lambeck, 2014).

Our analysis makes the simple assumption that subduction and collision-related forces act in a margin-normal sense (e.g., Faccenna et al., 2012; Iaffaldano & Lambeck, 2014). In the case of the subduction related forces, we are not particularly concerned with whether these forces represent 'net slab pull' *sensu stricto*, or other components of the subduction-related driving force: 'slab suction', trench GPE etc. While this type of analysis has a long history, the novelty here is to investigate how such margin-normal forces would contribute, respectively, to what we describe as the tangential and radial components of the net torque (as described in Section 3).

We address the limitations of this simple geometric analysis, by considering results from high-resolution global convection models (Hu et al., 2022). In such models, the plates and mantle are a single system: an incompressible continua subject to viscosity and bouyancy variations that depend on the thermal structure (among other factors). The flow is calculated based on global mechanical equilibrium, approximated with a Finite Element Method (Stadler et al., 2010). These models support the geometric analysis based on parameterised plate boundary forces. Specifically, they support our prediction of disproportionate impact of the IBM margin in the radial component of the Pacific Plate torque at ca. 47 Ma.

1.2 Zealandia and the Hikurangi Plateau

Along with changes in the Pacific Subduction margin, the Eocene tectonic reconfiguration involved development of a new Pacific-Australian plate boundary section transecting the rifted Gondwanan fragment of Zealandia. During the period ca. 47-32 Ma, the Euler Pole of the relative rotation between the Pacific and Australian Plates, was situated within or close to Zealandia (Sutherland, 1995; Keller, 2005). This configuration was expressed geologically in 'scissor tectonics' with extension in the southern Zealandia domain (Emerald Basin - Macquarie Ridge Complex), and convergence and shortening in the north (Sutherland, 1995; Keller, 2005; Stagpoole & Nicol, 2008).

The nature of the relative motion in this period led Reyners (2013) to propose that "resistance of the [Hikurangi] plateau to subduction had a first-order effect on plate motions...the western tip of the [Hikurangi] plateau appears to have acted as a pivot point on the plate boundary" (see also Eberhart-Phillips et al. (2018)). To elucidate this statement, we need to briefly outline the origin of Hikurangi Plateau (HP) and its proposed role on the evolution of Zealandia. This outline largely follows Reyners (2013); Eberhart-Phillips et al. (2018), and these studies provide additional details as well as visual summaries.

The HP emerged as part of the Ontong-Java large igneous province at ca. 120 Ma, which then separated into smaller plateau regions due to spreading ridge development (Mahoney et al., 1993). Based on the plate reconstructions considered in this study (e.g., Müller et al., 2016, 2019), the Hikurangi Plateau was part of a small, oceanic 'Hikurangi Plate' during the mid-Cretaceous. The Hikurangi Plate was located directly to the south of the Pacific Plate, and subducted southwards, centered on the Zealandia section of the Gondwanan continental margin. Collision and underthrusting of the HP with the margin of Gondwana occurred at about 90 Ma, leading to a rapid tectonic shift in the Southern proto-Pacific. Capture of the Hikurangi Plate by the NW moving Pacific Plate corresponded to a transition from subduction beneath Zealandia to rifting and Tasman Sea spreading in the continental back arc.

Tasman Sea spreading ceased during the Eocene plate reorganisation, and a new Pacific-Australian plate boundary emerged, comprising an intra-continental fault zone through Zealandia (Gaina et al., 1998). The architecture of the underthrust HP has been argued to control the localization of this boundary (Mortimer, 2018; Lamb et al., 2016). Finally, Reyners (2013) has proposed that resistance within this intra-continental plate boundary, may have had a 'first-order' effect on the relative motion of the Pacific and Australian Plates.

The proposed evolutionary sequence summarised here would constitute a remarkable, long-lived cascade of effects due to subduction collision and congestion. In this study we focus on the latter part of the sequence - the pivoting of the Pacific and Australian plates during the Eocene. We do not focus specifically on the Hikurangi Plateau, but more generally on the degree to which collision resistance along the Eocene Zealandia boundary could be expected to effect plate torques, relative to the effect of subduction margins (e.g., Whittaker et al., 2007; Faccenna et al., 2012; Hu et al., 2022).

1.3 Outline of the paper

- In Section 2 we highlight plate motion changes of the Pacific Plate in the period of interest, with particular attention to changes in both the tangential and radial components of the plate rotation.
- In Section 3 we provide the mathematical background and highlighting the origin and differences between the tangential and radial components of plate boundary generated torques.
- In Section 4 we show that during the Eocene transition, both the Zealandia boundary and the IBM subduction zone were well-oriented in terms of partitioning boundary-normal forces into CCW radial torques on the Pacific Plate.
- In Section 5 we estimate evolving torque components on the Pacific Plate, considering the contribution of subduction related forces as well as assumed collision resistance in Zealandia.
- In Section 6 we consider the dynamics of subduction initiation, and explore a simple *ad hoc* representation of these processes.
- In the Discussion we consider results from global geodynamic models, which reinforce the importance of the IBM in driving Pacific Plate radial rotation at 47 Ma. We consider the potential role of Zealandia under different assumptions, such as typical collision resistance forces inferred for present-day Earth.

2 Plate motion models

In this study we use recent global plate reconstruction models of the EarthByte Group (Müller et al., 2016, 2019), to address both the relative and absolute (i.e. relative to spin axis via a hotspot reference frame) motions of the Pacific and Australian plates during the Cenozoic, as well as to analyse parameterised plate boundary forces.

A significant source of (epistemic) uncertainty in the plate reconstructions relates to the structure and evolution of the NW-Pacific subduction margin in the Cretaceous and early Cenozoic. Recent studies propose a diversity of reconstructions, including potential intra-oceanic subduction zones that are not present in the reconstructions we utilise (Lin et al., 2022; Hu et al., 2022). The analysis carried out in this paper is subject to these uncertainties, increasingly-so for earlier stages.

The Cenozoic rotation poles of the Pacific and Australian Plates from Müller et al. (2016) are shown in Fig. 1. Note that the relative poles (red triangles) have been reconstructed into their past location as defined by the position of the Australian and Pacific Plates in the absolute reference frame (an Indo-Atlantic hotspot reference frame). The small symbols in Fig. 1 show the Euler poles prior to 47 Ma (red and green) and prior to 44 Ma (blue). There is a clear correspondence between the SE migration of absolute Pacific poles (green) and a similar jump in the relative Pacific-Australian poles (red).

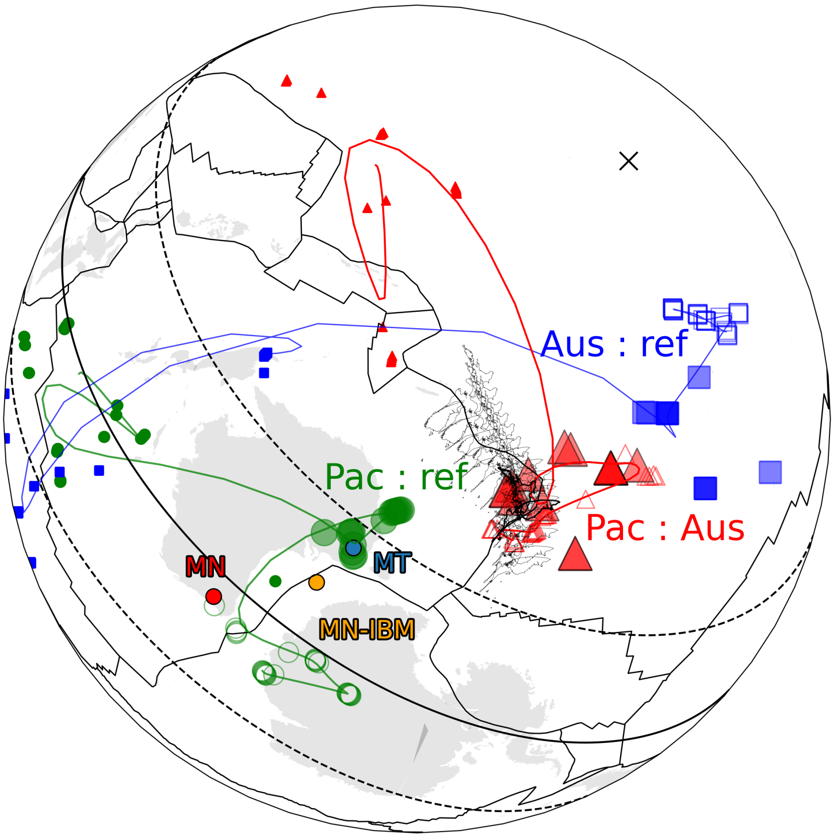

Figure 1. Cenozoic locations of Pacific and Australian Plate Euler poles. Location of plate boundaries (black lines) are shown for 47 Ma from (Müller et al., 2016). Green symbols: Pacific Plate relative to reference frame (Pac:Ref). Blue symbols: Australian Plate relative to reference frame. Red symbols: Pacific plate relative to Australian plate. Small filled symbols are pre-47 Ma poles (or pre 44 Ma for Aus:Ref), large filled symbols are 47-32 Ma poles (or 44-32 Ma for Aus:Ref). Open symbols are 32 Ma-present. Note that the relative poles (red triangles) have been reconstructed into their location as defined by the position of the Australian Plate in the absolute reference frame, at a given time. Coloured lines represent smoothed temporal paths, to help show the trajectory of the pole migrations. Migration of Zealandia is represented by the restored coastline locations. Bold coastline shows 47 Ma location. The black cross shows the average location of the Pacific plate centroid; circles represent planes drawn at $90° \pm 20$ relative to the centroid (solid and dashed respectively). A Pac:Ref Euler pole lying on the 90° circle corresponds to purely tangential motion at the Pacific Plate centroid. Three labelled circles show the calculated Euler poles at 47 Ma from different numerical models from Hu et al. (2022).

In terms of trying to quantify the role of tectonic forces in driving changes in plate motion, we focus primarily on the changes expressed in the absolute motion of Pacific Plate (for reasons that are elaborated throughout the manuscript). Fig. 2 (purple lines) shows several different components of the absolute Pacific Plate rotation during the Cenozoic: the azimuth, tangential magnitude and radial rotation at the centroid .

In this study we define the radial component of plate rotation as the component of the rotation vector in the direction of the plate centroid (e.g. Eq. 3). This measures the tendency of the plate to spin around an axis through its centroid. If we ignore the variations in the magnitude of the rotation vector (i.e. the angular velocity), the radial component can be expressed in terms of the angle between the centroid and the Euler pole (we discuss this representation further in Section 4). In Fig. 2, the radial component is shown as the deviation of this angle from 90°. When the resultant value is zero, the Euler pole is 90° from the centroid and there is no radial rotation at the centroid; when it is 90°, the plate simply spins around a radial axis at its centroid.

An important issue in recent geodynamic literature has been to understand the cause of rapid changes in the plate motion changes, such as the Eocene reorganization (Faccenna et al., 2012; Colli et al., 2014; Hu et al., 2022). Fig. 2 shows that such changes are present in both the tangential and radial components, as well as the magnitude of the Pacific Plate velocity (although apparently not always simultaneously across these components). The rapidity of such changes is suggested to be incompatible with the evolution of long wavelength buoyancy and flow in the mantle (Bercovici et al., 2000; Iaffaldano & Bunge, 2015). Such changes have often therefore been related to the evolution of force transmission through the plates and plate boundaries (England & Molnar, 2022; Hu et al., 2022). The current study is guided by these ideas.

Fig. 2 shows the major change in Pacific Plate rotation at 47 Ma, which includes the much-discussed westwards change in the azimuth of the tangential rotation component (Fig. 2A). Another important aspect of this transition, is the significant change in the radial component of the rotation (Fig. 2C-D). At 47 Ma, the total change in radial component is about 28° (+10° CW to -18° CCW) based on average values either side of the 47 Ma transition (shown with black dashed lines). The radial component of the Pacific Plate rotation remains high through 47-32 Ma, which we refer to as the 'pivot period'; this period sees the largest sustained radial rotation component of any stage during the Cenozoic. At about 32 Ma, the radial rotation component rapidly reverts to weakly CW, and has remained relatively stable until present.

The change in the location of absolute Pacific Euler Poles at 47 Ma brings them much closer to Zealandia, compared to their locations prior to 47 Ma (i.e. green symbols, Fig. 1, or black symbols in Fig. 2). It is clear that changes in both the tangential and radial components are involved in terms of moving the 47-32 Ma poles towards Zealandia. A similar SE migration of the relative poles (red symbols Fig. 1) suggests that changes in the absolute motion of the Pacific Plate at 47 Ma, strongly facilitate the corresponding change in the locations of the relative poles. This relationship cannot simply be assumed at the outset, as the relative Euler Poles could (in principle) be completely controlled by changes in the Australian Plate absolute motion. This does not seem to be the case.

The evolution of Pacific Plate Euler poles clearly depends on the choice of reference frame. The reference frame in Müller et al. (2016) represents a 'hybrid' approach, based on the approach of Torsvik et al. (2008) using a moving hot spot reference frame that takes mantle convection into account. Supplementary Fig. S5 shows a number of different reference frames based on different hotspot reference frames, including the fixed Pacific hotspots that are used to define absolute motion in Wessel and Kroenke (2008). All of these reference frames show the same overall pattern, with a SE migration of the poles, along with a radial excursion in the period 47-32 Ma. See the caption for Fig. S5 for further details. We note that in the 'hybrid' reference frame implemented in Müller et al. (2016), the distinctive bend in the Hawaiian–Emperor seamount chain is attributed to a combination of hotspot drift and non-trivial absolute plate motion change.

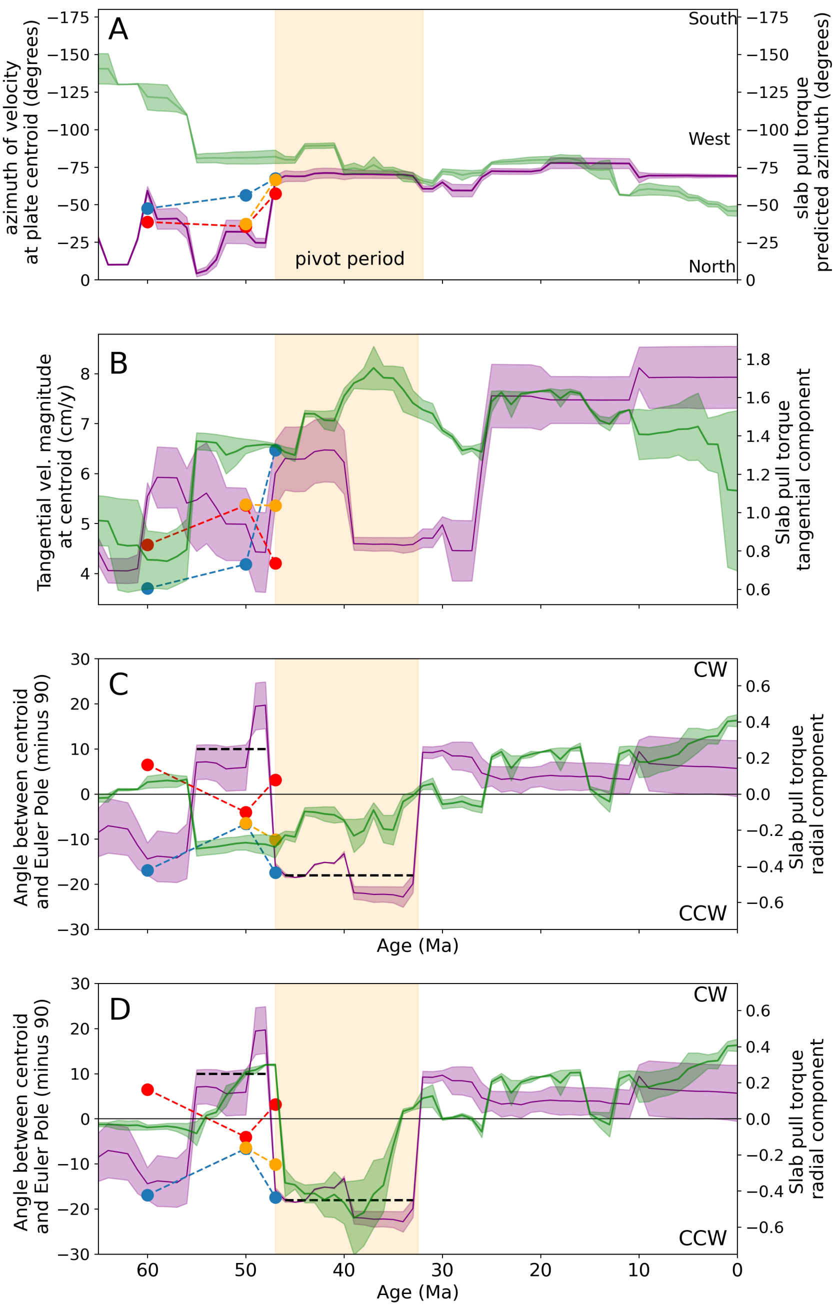

Figure 2. Comparison of Pacific Plate motion trends (purple – left hand axes) and estimated slab pull torques (green – right hand axes); The shaded regions represent the span of estimates from two reconstruction models (Müller et al., 2016, 2019): A) shows the azimuth of the velocity at the centroid (purple), versus azimuth predicted by the net slab pull torque (green), assuming uniform plate boundary normal force. Note that in the early Cenozoic, there is significant misalignment between these quantities ($\sim 90^\circ$); B) shows the magnitude of the tangential part of the Pacific rotation vector at the centroid (purple) and the (dimensionless) tangential component of the slab pull torque (green); C) and D) show the radial rotation component, measured in terms of the angle of the Euler pole relative to a 90° great circle around the centroid (purple), and the (dimensionless) radial component of the slab pull torque (green). D) in this panel the radial component of the slab pull torque (green) includes an simple representation of subduction initiation dynamics (see Section 5), resulting in a lag between IBM initiation (55 Ma in the plate reconstruction) and the effect on radial rotation at 47 Ma.

3 Torques due to plate boundary forces

3.1 General case

Because plate motion is restricted to the surface of a sphere, the 6 degrees of freedom that apply to rigid body motion, can be reduced to 3 rotational components (Forsyth & Uyeda, 1975; Bird et al., 2008). The equilibrium problem is then to understand the balance of torques that give rise to observed rotations. For plate motions, rotations are commonly expressed in terms of a rotation axis (Euler Pole) and angular velocity, or simply a rotation vector ($\vec{\omega}$).

The rotations and torques are naturally described with respect to the center of the earth, and hence the radius of the earth enters the description as the moment arm length. For instance, in terms of parameterised plate boundary forces (Forsyth & Uyeda, 1975; Becker & O'Connell, 2001), the torque vector component due to a plate boundary normal force, over a small section of trench, may be written as:

$$d\vec{\tau} = F_n(\vec{r_0} \times \hat{n})dl \tag{1}$$

Where F_n is the (scalar) normal force density (force per unit length, expressed in this study in units of TN/m), $\hat{n}$ is a unit vector in the local tangent plane that is normal to the plate boundary, and $\vec{r_0}$ is the radius vector that points to the location of the plate boundary. The total torque due to plate boundary normal forces is:

$$\vec{\tau}_{\text{net}} = \sum F_n(\vec{r_0} \times \hat{n})dl \tag{2}$$

Eq. 2 represents a typical description used to investigate mechanical equilibrium of rigid plates on a sphere (Forsyth & Uyeda, 1975; Becker & O'Connell, 2001). However, this description tends to obscure an important aspect of the mechanics, which is that the torque vector described by Eqs. 1 and 2, conflates two kinds of torques. The distinction between these types of torques is closely related to the more familiar case of the motion of a solid object constrained to a planar surface. As we will show, the mechanical descriptions converge for very small plates (which are approximately planar). Fig. 3 attempts to clarify these relationships. We will hereafter condense the notation by denoting the point force along a small boundary increment (dl) as $\vec{F_n} = F_n dl \;\; \hat{n}$, and dropping the differential symbol, so that Eq. 1 can be written as:

$$\vec{\tau} = \vec{r_0} \times \vec{F_n} \tag{3}$$

Fig. 3 shows the effect of an arbitrary point force $\vec{F_n}$ acting on a square plate confined to (a) a planar surface and (b) the surface of a sphere. In each case the point force acts at the corner of the square plate, in the direction given by the dashed edge (and hence normal to the adjacent edge), as shown by the green arrows. In each case, the point force vector is also decomposed into components that are parallel (blue) and orthogonal (brown) to the centroid direction, which is shown with the blue line / great circle arc. In both cases the z axis is aligned with the vertical direction at the centroid of the plate (or center of mass).

In the planar case (a) the distinction between the net force and the torque is straightforward. A torque arises because the point force *is not* parallel to the centroid direction (shown by the blue line). This torque is given by $\vec{r} \times \vec{F_n}$, or $|\vec{F_n}||\vec{r}|sin(\theta)\hat{z}$. The black arrow, which is orthogonal to the centroid direction, shows the component of the force that produces the torque around the z axis, with a moment arm $\vec{r}$. The net force in (a) is $\vec{F_n}$.

For a rigid body on a planar surface (a), pure translation requires that the point force is parallel to the centroid direction. In this case the net force has no dependence the length $\vec{r}$. Pure rotation requires a force distribution such that the torques are complimentary, but the net forces cancel. A 'double couple' is the simplest example. These end-member cases require very specific force distributions: any arbitrary force distribution along the boundary is expected to give rise to a combination of translation and rotation, and can be represented by a combination of an equivalent net force at the centroid, as well as a torque produced by an appropriate double couple.

In the spherical case (b) the point force $\vec{F}_n$ is assumed to contribute to a driving torque τ, as given by Eqs. 1 or 3. We can decompose this torque into components around each of the (Cartesian) axes shown in the figure. The moment arms associated with each of these components are shown with the blue, brown and black dashed lines. Consider first the component of the torque associated with the force parallel to the centroid direction (blue arrow). For the configuration shown in (b), this component of the torque vector is parallel to the x axis. The moment arm length is r_0, it has no dependence on the location of the point force (which is analogous to the planar case in(a)). This component of the driving torque produces purely tangential motion at the centroid, because $\hat{r}_c \times \hat{x}$ is tangent to the surface, where $\hat{r}_c$ is a unit vector that points radially outward at the centroid. For the configuration shown in (b), $\hat{r}_c \equiv \hat{z}$.

Next consider the component of the torque in (b) that acts in the centroid direction (z or $\hat{r}_c$). This represents the component of a torque vector that tends to spin the plate around centroid. We refer to this as the radial component of the torque. This radial component of the torque has a moment arm length of $r_0 \sin(\phi)$ where ϕ is the angle between the centroid and the boundary where the force is located. As in the planar case, this component of the torque has an intrinsic dependence on the distance between the point force and the centroid (or z axis). Note that in the case of a very small plate, we can use the small angle approximation ($\sin(\phi) \approx \phi$) in which case, the z component of the torque depends on $r_0\phi \approx y$, i.e the torque is simply proportional to the distance from the z axis, as in the planar case.

The brown arrow shown in (b) is the component of the force that gives rise to the torque component around the y axis. This also produces purely tangential motion at the centroid. Again, this is analogous to the effect of the net force in (a), given by the component of force acting orthogonal to the centroid direction. The moment arm length is given by $r_0 \cos(\phi)$, or by r_0 in the small angle approximation.

With reference to Fig. 3b, we can associate the x, y, z axes with the unit vectors:

$$
\begin{aligned}
\hat{x} &= \hat{r}_0 \times \hat{r}_c \\
\hat{y} &= \hat{r}_c \times (\hat{r}_0 \times \hat{r}_c) \\
\hat{z} &= \hat{r}_c
\end{aligned}
$$

As shown in Fig. 3, the radial and tangential components of the torque can be written in terms of angle between the plate boundary normal and the centroid direction (θ) and the angle between the plate boundary point force and the centroid (ϕ):

$$
\begin{aligned}
\vec{\tau}_{\mathrm{rad}} &= |\vec{F}_n| r_0 \, \sin(\theta) \, \sin(\phi) \, \hat{z} \\
\vec{\tau}_{\mathrm{tan}} &= |\vec{F}_n| r_0 \, \cos(\theta) \, \hat{x} \\
&\quad + |\vec{F}_n| r_0 \, \sin(\theta) \, \cos(\phi) \, \hat{y}
\end{aligned}
\tag{4}
$$

The tangential component of the torque can also be described by an equivalent force acting at the centroid (e.g., Becker & O'Connell, 2001):

$$\vec{F}_{eq} = (\hat{r}_c \times \vec{\tau}_{\tan})/r_0 \tag{5}$$

Because the surface of a sphere is locally flat, the description of the spherical case must be identical to the planar case for a small plate. If we apply the small angle approximations (for ϕ) to the tangential components of the torque, and noting that the cross products in Eq. 5 simply switches the x and y axes, the net force at the centroid can be written:

$$\begin{aligned}\vec{F}_{eq} &= (\hat{r}_c \times \vec{\tau}_{\tan})/r_0 \\ &= |\vec{F}_n|\ \cos(\theta)\ \hat{y} \\ &+ |\vec{F}_n|\ \sin(\theta)\ \hat{x}\end{aligned} \tag{6}$$

Which is identical to expression for $\vec{F}_{\rm eq}$ for the planar case shown in Fig. 3a. A similar equivalence applies in the case of the radial component of the torque. Based on these considerations we refer to the tangential and radial components of the torque vector as fictitious and true torque components.

For the radial component of plate driving/resisting torques, the magnitude of the torque depends on two aspects of the geometry: the azimuth of the plate boundary relative to the centroid (i.e. the component of the force that is normal to the centroid direction ($\sin(\theta)$), and also the angle (distance) between the plate centroid and the boundary ($\sin(\phi)$). Hence, plate boundary normal forces that are perpendicular to the centroid direction, and are a long way from the centroid (i.e. $\sin(\phi), \sin(\theta) \rightarrow 1$) have the greatest potential to impact the radial component of torque. Of course, large ϕ implies a large plate, and the area increases more rapidly ($\mathcal{O}(\phi^2)$) than the moment arm length of the torque ($\sin(\phi)$). If basal drag plays an important role in resisting plate boundary forces, then large plates will exhibit less sensitivity to radial torques, even though the net radial component may be higher than in the case of small plates. At the present day, there are 2 'rigid' plates with anomalously high radial rotation: the Cocos and Philippine Sea Plates (e.g., Becker & O'Connell, 2001). This observation is consistent with the idea that net radial torques from the plate boundaries may be balanced by basal drag, with small plates requiring significantly higher radial rotations to achieve such a balance.

In the following section we extend these generic ideas to the case of the Zealandia and the IBM margin in the Eocene.

3.2 Pacific Plate at 47 Ma

The concepts outlined in the previous section are now extended to the Pacific Plate boundary during the Eocene transition period. The purpose of this section remains primarily conceptual; the actual estimation of torques based on plate tectonic reconstructions is presented in Section .

Fig. 4 shows the tectonic configuration at 47 Ma, rotated so that the Pacific Plate geometric centroid lies along the z axis of a Cartesian coordinate system, and so that the great circle arc that connects the centroid to a point on the IBM trench, is parallel to the y-axis (the great circle arc is shown with a thin blue line). This rotation places the Pacific plate, and the IBM trench, into a similar configuration as shown in the generic case (square plate) in Fig. 3b. The left hand panel of Fig. 4 shows the outline of the plate boundaries as well the evolution of the absolute Pacific plate Euler poles during the Cenozoic.

In the right hand panel of Fig. 4, the force due to slab pull at the IBM is represented as a point force acting in a margin normal direction (shown schematically with

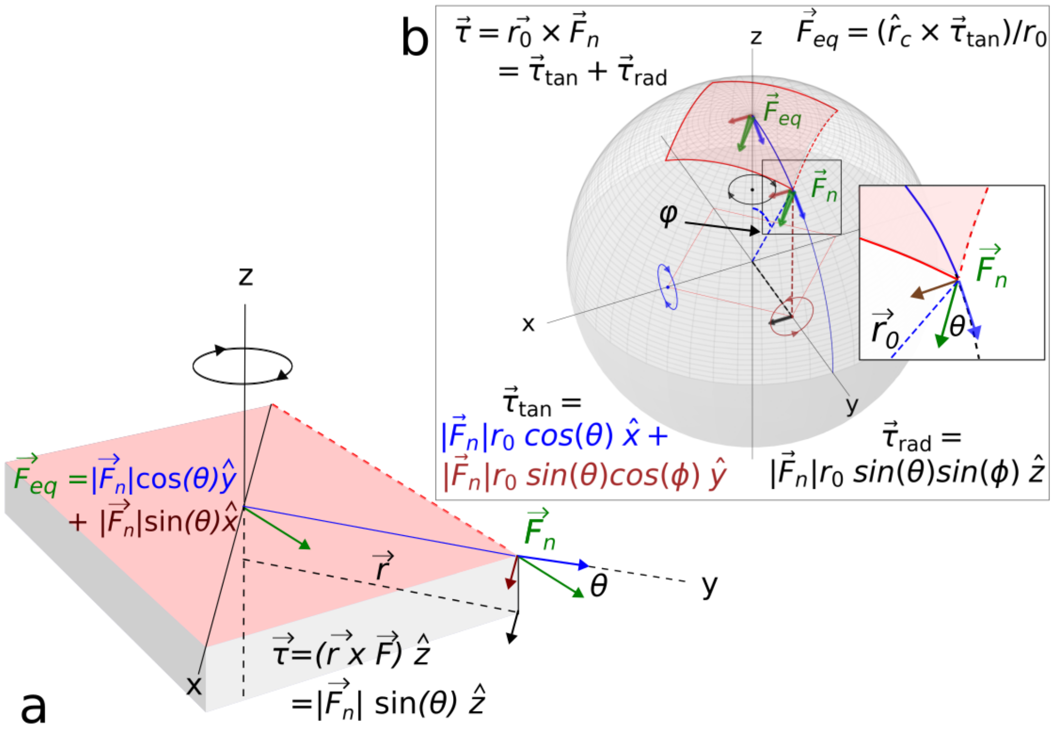

Figure 3. Effect of an arbitrary point force $\vec{F}_n$ acting on a square plate confined to (a) a planar surface and (b) the surface of a sphere: (a) shows the familiar case of a point force acting on a rigid body, contributing to a net force and a torque around the center of the object. $\vec{F}_n$ acts at the corner of the square plate, in a direction parallel to the edge of the square outlined with the dashed red line, and normal to the adjacent edge. The blue and brown arrows show the components of the force that are parallel and perpendicular to the centroid direction. The components of the net force ($\vec{F}_{\mathrm{eq}}$), and the torque (τ) are written as a function of θ, the angle between the point force on the boundary and the centroid direction; (b) shows the equivalent situation for a square plate on the sphere. Here the point force $\vec{F}_{eq}$ is associated with a torque (τ), as in Eq. 3. This torque has components in the x, y, and z directions. The z direction is aligned with the vector that points radially outward at the plate centroid ($\hat{r}_c$). We refer to the component of the torque in the z (or $\hat{r}_c$) direction, as the radial component of the torque; this is the true torque component, which analogous to the usual definition of the torque as in case (a). For small plates (where the small angle approximation for ϕ is valid), the descriptions of the mechanics in (a) and (b) are identical, as discussed in the main text.

Parameter name	**Type**	**Symbol**	**Units**
Earth mean radius	scalar	r_0	km
Earth radius vector	vector	$\vec{r}_0$	km
Earth radius unit vector	vector	$\hat{r}_0$	-
Plate boundary normal vector	vector	$\hat{n}$	-
Plate boundary normal force density†	scalar	F_n	TN/m
Plate boundary normal point force	vector	$\vec{F}_n$	TN
Plate centroid unit vector	vector	$\hat{r}_c$	-
Angle btw $\hat{n}$ & centroid direction	scalar	θ	rad.
Angle btw boundary point & centroid	scalar	ϕ	rad.
Rotation vector	vector	$\vec{\omega}$	°/Ma
Radial rotation unit vector ‡	vector	$\hat{\omega}_{\text{rad}}$	°
Angle btw centroid and Euler Pole	scalar	γ	°

Table 1. Quantities and symbols used in the paper. † We discuss both dimensionless and dimensional values for plate boundary normal forces. Where dimensional values are used, the units are TN/m, or TN. ‡ See Section 4 for a description of units and how $\hat{\omega}_{\text{rad}}$ is visualised.

a green arrow). As in the previous section, this point force is decomposed into components parallel (blue) and orthogonal (brown) to the centroid direction. These components of the point force generate torques around the x and y axes respectively, with moment arms shown with the dashed lines in the same colors. Likewise, the black arrow, which is the projection of the brown arrow on the hemispheric plane ($z = 0$), is the component of the point force that is responsible for the true torque – the rotation around the centroid vector (in this configuration the z axis).

The net torque vector associated with slab pull at the IBM trench at 47 Ma is shown with the green double-ended arrow at the centroid location (pole) in Fig. 4. This net torque vector is based on the actual summation of incremental torques based on the 47 Ma boundary configuration of Müller et al. (2016). The dashed green line shows the total tangential component of the torque vector, which contains the contributions of the two components ($\hat{x}$ & $\hat{y}$) described in Eq. 4. The full torque vector is also decomposed into rotations around the three axes, shown in blue, brown and black; the relative size of these torque components is shown to scale. One can see that the radial component (black) is of similar magnitude to the components that contribute to the tangential torque (blue and brown).

In addition, Fig. 4 shows the orientation of a boundary-normal collision resistance force at Zealandia (shown schematically with the red arrow). To simplify the figure, we have not shown the full decomposition of this point force, but only the projection of the point force onto the hemispheric plane (also with a red arrow). This evidences the capacity for a plate boundary normal force at Zealandia to produce a radial component of torque, primarily because angle between the centroid direction and the boundary normal (i.e. θ) is large. Again, this is a schematic representation that is designed to highlight how the geometry of the boundaries is related to the capacity to generate radial and tangential torque components.

The key insight from Fig. 4 is that plate boundary normal forces along the IBM trench and Zelandia, both have a relatively large capacity to influence the radial torque components. In addition, the radial torque components are complimentary – both having a CCW sign (when looking down on the Pacific centroid). In fact, these two boundaries act in the sense of a double couple, as the tangential component of collision resistance along Zealandia tends to oppose the tangential component of torque due to the IBM. However, this statement does not imply that the 2 margins would act as a perfect double couple, as the relative size of the plate boundary forces, and hence the torques is unknown (and will depend on further assumptions). This point is discussed further in the following section, and highlighted in Fig. 5.

3.3 Estimation and visualisation of torque components

Having discussed the general aspects of torques due to plate boundary forces, we conclude this section with some methodological details in applying this framework to plate reconstruction models. In this study we restrict our attention to the plate boundary normal forces that arise from Pacific Plate subduction, as well as the potential collision resistance from the intra-continental Zealandia boundary. Eq. 4 provides a means of calculating the radial and tangential components of the torque, in a rotated reference frame. This is instructive for the case of a specific plate boundary point force, but is inefficient for analysing the effect of extended boundary segments. Instead, to calculate torque components due to Pacific Plate subduction, we first calculate the net torque (τ_{net}) as the sum of torque increments, as in Eq. 2. Having calculated a net torque vector (τ_{net}) in a fixed Cartesian reference frame, we derive the radial and tangential components by simply taking the dot product of the net torque with the unit vector that points radially outward at the plate centroid ($\hat{r}_c$). We compute the torque components both in terms of the total subduction related torque from Pacific Plate Slabs, and at the level of individual trench segments (e.g. IBM, Tonga, Aleutian etc.). Fig. 5 shows the results of this analysis applied to the evolving subduction margin of the Pacific plate, based on the plate reconstructions of Müller et al. (2016, 2019).

Our analysis does not account for the age of the subducting plate in terms of the predicted slab pull force, and is purely based on the geometric information. In keeping with this assumption, our calculations are based on the geometric centroid of the (Pacific) Plate, rather than attempting to estimate the center of mass. The torque values in Fig. 5 are non-dimensionalised by assuming a reference torque $\tau_{\text{ref}} = F_n {R_e}^2$. The torque calculations (e.g Eq. 1) are scaled by τ_{ref}, such that the magnitude of F_n is not actually specified in our calculations; again the values plotted in Fig. 5 represent geometric information only. To recover a dimensional torque from the values shown in Fig. 5, one would multiply by τ_{ref}. For instance, if a boundary normal force of 5 TN/m were assumed, a dimensionless torque magnitude of 1 would equate to torque magnitude of about 2×10^{26} Nm. If this value represented the tangential component of the torque, it could be described as an equivalent force of $\approx 3.2 \times 10^{19}$ N acting at the centroid.

To estimate the torque contributions due to collision resistance at Zealandia, we have made a few simplifying assumptions. We model the collisional boundary during the pivot period (ca. 47-32 Ma), as a 1000 km segment which is perfectly parallel to the centroid direction. This means that the plate boundary normal force is orthogonal to the centroid direction, or $\theta = 90°$ (see Fig. 4). The main reason for the simplified approach is that the precise length of the the boundary that might contribute to a collisional resistance force is uncertain. The length of intra-continental boundary, parallel to the centroid direction, is on the order of 1000 km, as shown in Supplementary Figure S2.

The same process is used the decompose the radial and tangential components of the Pacific plate rotation vector ($\vec{\omega}$):

$$\begin{aligned} \vec{\omega}_{\text{rad}} &= \vec{\omega} \cdot \hat{r}_c \\ \vec{\omega}_{\text{tan}} &= \vec{\omega} - \vec{\omega}_{rad} \end{aligned} \tag{7}$$

Note that when a plate rotation is purely tangential (at the centroid), the rotation axis is orthogonal to the centroid vector, and hence the Euler Pole of the rotation lies at 90° from the plate centroid; the finite rotation at the centroid is then a great circle arc. In contrast, the plate rotation is purely radial when the Euler pole lies at the plate centroid; in which case the plate spins about the radial axis.

The radial and tangential rotation components expressed in Eq. 7 will clearly depend on the magnitude of the rotation vector $\vec{\omega}$. However, if we consider only the orientation of $\vec{\omega}$, (i.e. $\hat{\omega}$), then the radial component of rotation can be approximated as an angle:

$$\hat{\omega}_{\text{rad}} = \cos(\gamma) = \sin(\frac{\pi}{2} - \gamma) \approx (\frac{\pi}{2} - \gamma) \tag{8}$$

where γ is the angle between the Euler Pole and the centroid. In Fig. 2C&D we use the value of $\frac{\pi}{2} - \gamma$ to represent the radial component of the rotation (making use of the small angle approximation). This has the advantage of providing a intuitive geographic representation of the radial component, which is the angle between the Euler Pole and a great circle drawn at 90 ° from the centroid. Hence, in Figs. 1 & 4, the Pacific Plate Euler poles can be seen to deviate from the 90 ° great circle, particularly during the period 47-32 Ma (i.e. the pivot period). Supplementary Fig. S4 shows a comparison between the approximation of the radial component ($\frac{\pi}{2} - \gamma$) and the true radial component ($\vec{\omega}_{\text{rad}}$, in units of °/100 Ma).

In the following sections we will refer to the relative magnitude of plate boundary force densities (e.g. TN/m) that might arise from net slab pull F_{sp}, versus those that arise from the Zealandia collisional boundaries F_c. We denote the ratio as $F_R = F_c/Fsp$.

4 Evolution of torques due to Pacific Plate boundary forces

There is a long-standing view that the c. 47 Ma change in Pacific Plate motion may be related to plate boundary reorganization, in particular of subduction margins (Whittaker et al., 2007; Faccenna et al., 2012; Sutherland et al., 2017; Hu et al., 2022). Although the overarching problem addressed in this study concerns the relative motion between the Pacific and Australian plates, our analysis is focused mainly on the changes in the absolute motion of the Pacific plate throughout the Cenozoic (for reasons discussed in Sections 1 & 2). In this section we focus on reconstructions of the evolving Pacific subduction margin, and in particular, how this evolution might be reflected in terms of the radial component of the subduction-related torque. We also estimate the effect of collision resistance along the Zealandia boundary, as discussed in the previous section.

Fig. 5 shows the radial and tangential torque components, based on the geometric information from plate reconstructions. The solid black lines in Fig. 5 show the estimated total (Pacific-wide) torque components due to trench normal slab pull. Note that the total tangential torque (Fig. 5A) is the *vector sum* of the boundary contributions, it is not the sum of the magnitudes of those components, nor is it the sum of the magnitudes of the trench segments (e.g. IBM, Tonga, etc., shown with colored circles Fig. 5). This is simply because the torque vectors of different subduction segments are generally not parallel. In fact, the total tangential subduction-related torque estimated for the Pacific plate, averages about 50-60 % of the sum of the magnitudes of the individual components; this means that of the total subduction boundary of the Pacific plate, there is only about a 50-60 % constructive contribution. This has implications for arguments about the value of trench length to plate area (Hager & O'Connell, 1981; Forsyth & Uyeda, 1975), which is already much lower for the Pacific Plate than for other oceanic subducting plates (e.g. Nazca and Cocos).

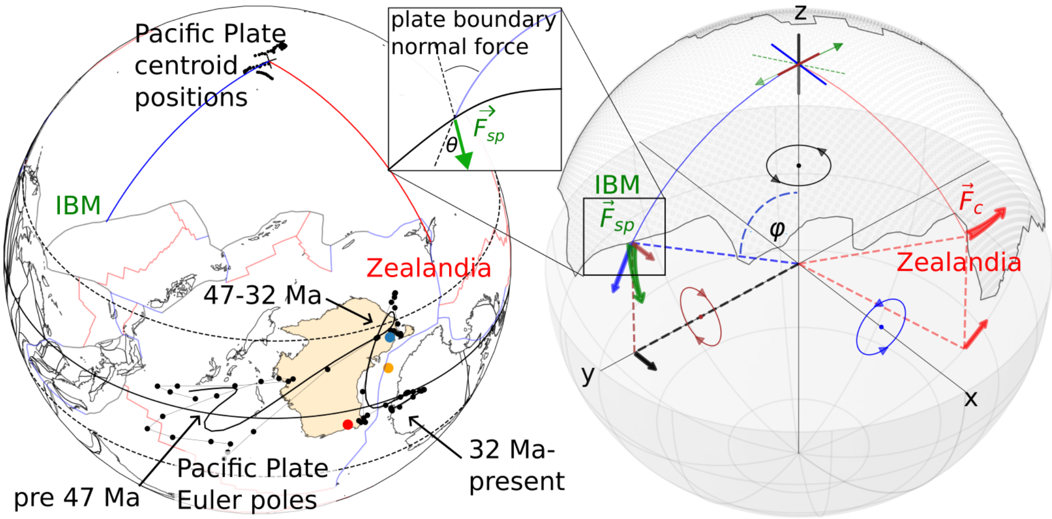

Figure 4. Schematic showing how different torque components are generated from plate boundary forces. Both panels show the tectonic configuration at 47 Ma. Globe is rotated so that the Pacific centroid lies at the pole (along the z-axis) while the arc from the centroid to the IBM trench is parallel to y-axis. Left panel shows the Pacific Plate Euler poles relative to the reference frame (black points). The right panel shows a schematic representation of plate boundary normal forces: for subduction at the IBM (green) and collision resistance at Zealandia (red). The blue, brown and black arrows show how the IBM plate boundary normal force contributes to three orthogonal torques. The component of force parallel to the centroid direction (and the y-axis) produces a torque around the x-axis (blue symbols). This is a psuedo-torque because it has no dependence in the angle ϕ. The component of the force orthogonal to the centroid direction produces a radial torque (a 'true' torque) around the z-axis (or centroid axis). Both the IBM and Zealandia are expected to produce CCW radial torques on the Pacific Plate.

In the plate reconstruction of Müller et al. (2016) there is a significant increase in Western Pacific subduction zone length at about 55 Ma, associated with the initiation of IBM and Kurile segments. This is reflected in a significant increase in the total tangential component of the slab pull torque at 55 Ma, shown with the solid black line in Fig. 5A. For the rest of the Cenozoic, the predicted magnitude of the tangential torque component relatively stable, with an average dimensionless value of around 1.4.

Fig. 5B shows the radial component of the estimated torque. At the beginning of the Cenozoic, the predicted radial component of the torque is negligible. Overall, there is a trend from a predicted CCW slab pull radial torque from 55-32 Ma, to a CW slab pull radial torque from 32 Ma - present. This broad trend is reflected in radial component of the (absolute) Pacific plate motion (e.g. Fig. 1) although the variations that are present in the plate reconstruction models are generally more abrupt than the slab pull contributions would predict.

At this stage, the most important takeaway from the analysis shown in Fig. 5B, is the importance of the IBM trench in terms of the predicted radial torque component. Within the period of 47-32 Ma, the radial component of the IBM torque is more than twice that of the next highest subduction segment (Aleutian). This is in contrast to the magnitude of the tangential torque component, where the IBM produces a comparable magnitude to other segments.

The red lines in Fig. 5, show estimates for the contribution of Zealandia collision resistance, based on the assumptions outlined in Section 3.3. The dashed red lines in Fig. 5 show the estimated torque contributions for Zealandia, when the magnitude of the plate boundary normal force density (F_n: TN/m) is assumed to be the same as that of the subduction boundaries (i.e. $F_R = 1$). Again, we see that Zealandia has a relatively high radial torque component compared to the tangential component. For the assumption that $F_R = 1$, collisional resistance along Zealandia amounts to about 1/3 of the radial torque produced by IBM. This is mainly a reflection of the length of the 2 boundaries, with the IBM trench being about 4.5 times longer than the assumed Zealandia collision length. The fact that Zealandia segment is sub-parallel to the centroid direction, partially compensates for the length difference, through the $\sin(\theta)$ dependence described in Eq. 4. The dot-dashed red line shows the estimated contribution of Zealandia if the magnitude of the plate boundary normal force is 3 times higher than the subduction margins (i.e. $F_R = 3$). In this case the CCW radial torque contribution from Zealandia is similar to that of the IBM during the pivot period (Fig. 5B). We revisit these assumptions in Section 5. The dashed and dot-dashed black lines in Fig. 5 show the combination of the total subduction related torques, with the torque from Zealandia, assuming $F_R = 1$ and $F_R = 3$. Note that the radial components are complimentary while the tangential components are opposed.

In terms of the ratio of the radial to tangential components of the torque vector, the IBM margin has a predicted maximum Cenozoic value of almost unity (~ 0.9, at 45 Ma). In comparison, averaged across the entire Pacific subduction system, this ratio has an average Cenozoic value of only 0.09, and a maximum value of 0.25. This maximum occurs at present day, a reflection of the fact that the radial torque components of all Pacific margin subduction segments are currently atypically complimentary, dominated by CW components (as shown in Fig. 5). Meanwhile, under the assumptions outlined above, the 47 Ma intra-continental Zealandia boundary, has a radial/tangential ratio of ~ 1.5 (from Eq. 4 this ratio is equal to $\cos(\phi)/\sin(\phi)$, and corresponds to ϕ of 56 °). From a purely geometric standpoint, Zealandia has the highest propensity to effect radial torques (for a given component of boundary normal force). The IBM margin (particularly around 45 Ma), also had a large radial torque efficiency, when compared with the average across the entire Pacific subduction margin.

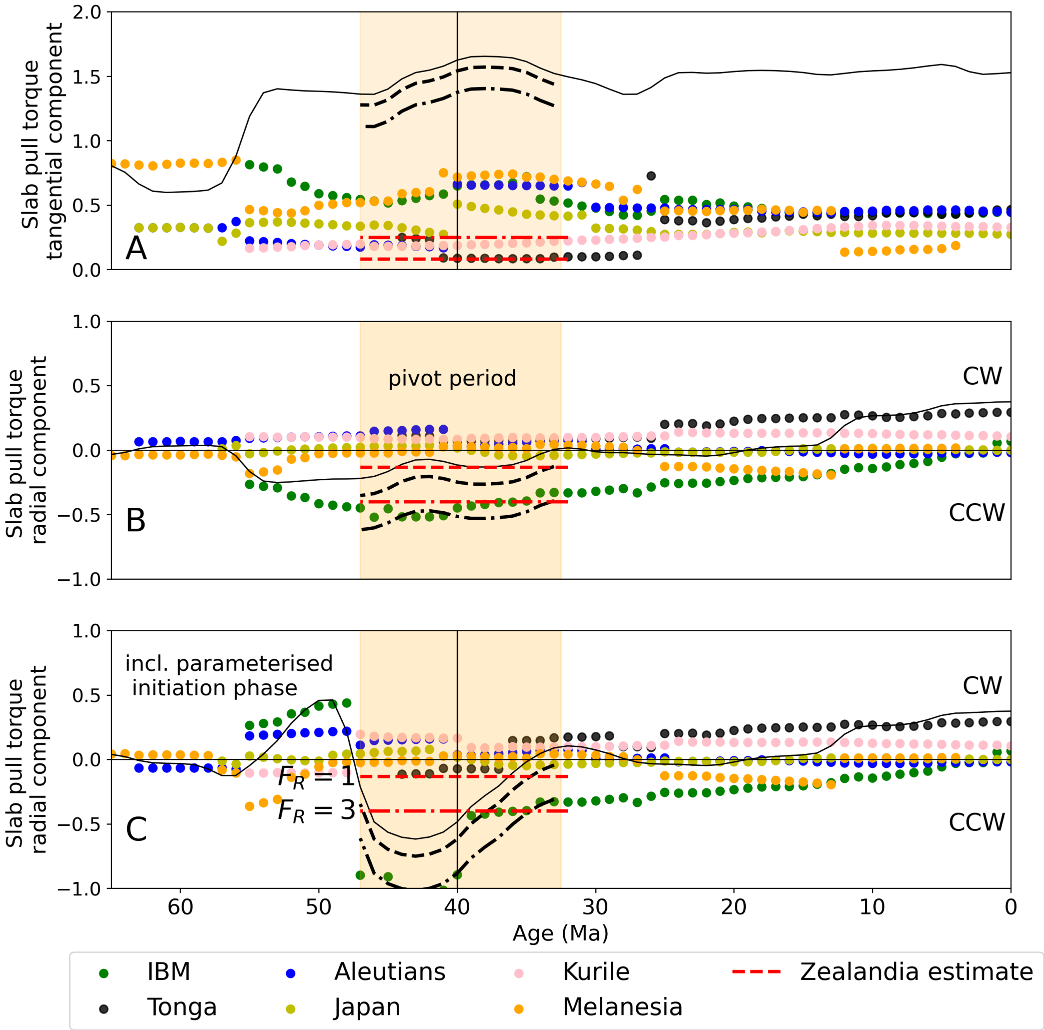

Figure 5. Evolution of torque components due to Pacific slabs (colored dots) and the total slab pull torque (solid black lines). Red lines show estimated torque contributions due to collision resistance at the Zealandia boundary, assuming collision force densities equal to slab pull ($F_R = 1$ dashed red line), and three times slab pull ($F_R = 3$ dot dashed red line). The dashed and dot-dashed black lines show the potential combined contribution from slabs and Zealandia. Note that radial torques are complimentary and the tangential torques are opposed (although the partitioning is not equal). A) shows tangential torque components; B) shows radial torque components; C) shows radial torque components with a simple representation of subduction initiation dynamics applied to the slab pull torques, as discussed in Section 5.

5 Timing and evolution of subduction initiation

In the previous section we highlighted the potential link between IBM subduction and the increase in CCW radial rotation of the Pacific plate that occurs at 47 Ma. An obvious limitation of this model is the lag between the IBM initiation time (55 Ma) in the reconstruction of (Müller et al., 2016) and the corresponding change in Pacific plate motion (47 Ma).

This issue has also been highlighted in the recent study of Hu et al. (2022). That study focused on the drivers of the rapid change in the azimuth of the Pacific plate (effectively the tangential part of the rotation). They argued that new evidence suggests a somewhat later IBM initiation phase (51 Ma), while the force of the slab is not actually felt for another 4 Myr, representing the time taken for the slab pull to begin to dominate over forces resisting subduction (such as bending, interplate friction etc.)

Along similar lines, we modify our analysis to capture a simple *ad hoc* representation of the dynamics of subduction initiation. This tries to capture 2 main processes, motivated by previous studies. The first process relates to the anticipated conditions of compressive stress across the margin during early stages of subduction (Cloetingh et al., 1989; Gurnis et al., 2004). The second process is informed by geodynamic models which show that the fastest subducting plate velocities and highest slab pull forces will be generated shortly before the slab interacts with the a higher-viscosity transition zone (Garel et al., 2014; Holt et al., 2015).

In order to explore a simple realisation of these processes, we modify the Pacific Plate subduction torques in the following way: 1) we choose a time representing the total initiation phase, i.e. the time from the onset of convergence, through to anticipated interaction with the slab with the lower mantle; 2) we then modify the torques such than in the first half of this period, the plate boundary acts as a resisting component in the plate torque balance, while in the second half of the initiation period, the plate acts a driving force, with a value of twice the reference slab pull force (which for Fig. 5 is unity due to the values being non-dimensional).

Fig. 5D shows the estimated radial torques when this simple representation of subduction initiation dynamics is included. The total initiation phase time reflected in Fig. 5D is 16 Ma, and was arbitrarily chosen to try to align the estimated radial torque signal with the 47 Ma change in Pacific plate motion. The duration is not unreasonable however, being comparable to the upper mantle transit time, assuming 45° dip, and a velocity imposed by the typical rate for Pacific plate (e.g. 6 cm/y). Of course, recent studies have advocated for a slightly later onset time of 51 Ma for the IBM (Hu et al., 2022), in which case somewhat a shorter initiation phase time could be accommodated.

The exercise simply demonstrates that general insights about of the dynamics of subduction initiation processes help to account for both the lag, and the magnitude of change in the CCW radial rotation of the Pacific Plate at 47 Ma. Based on these assumptions, the changes in subduction related torque at around 47 Ma are now even more strongly linked with the IBM margin, which first acts as a resisting force on the Pacific Plate ($\sim$ 55-47 Ma), and then contributes twice the net slab pull ($\sim$ 47-39 Ma) relative to when the slab is assumed to be fully supported in the lower mantle. In Fig. 2D, we show the predicted radial component of the slab pull torque with parameterised subduction initiation, which correlates fairly closely with the radial rotation component of the Pacific Plate from the plate reconstruction models (Müller et al., 2016, 2019) reconstruction (shown in purple).

6 Discussion

6.1 Insights from global geodynamic models

Even when modified to try to better represent dynamic process (such as subduction initiation), the use of parameterised plate boundary forces has obvious limitations (Becker & O'Connell, 2001). The results from dynamic computational models provides an alternative route to try to establish potential links between evolving plate boundaries, and plate motion changes. Computational methods have now developed to the point where it is possible to model global-scale flow, at sufficient spatial scale to capture the coupled plate-mantle system including plate boundaries at the kilometer scale.

A recent example of this approach is demonstrated in Hu et al. (2022), which compares two alternative models for the subduction boundary evolution of the Pacific Plate. The motivation for that study is to understand the rapid change in motion (particularly the azimuthal change) at 47 Ma. Such models are dependent on an assumed plate reconstruction model, as this establishes, for instance, the upper mantle density structure as well the location of the weak plate boundaries (e.g., Hu et al., 2022; Stadler et al., 2010).

The reference model ('MT') presented in Hu et al. (2022) is based on the plate reconstruction of Müller et al. (2016), the same model as we use in this study to evaluate torques due to plate boundary forces. An alternative model ('MN') includes a several-thousand kilomter north-dipping intra-oceanic 'Kronotsky' subduction, which is active until 50 Ma. They also test this alternative model with ('MN-IBM') and without ('MN') the IBM system. It should be noted that in all of these alternative models, the lithospheric structure includes the new plate boundary through Zealandia (from 47 Ma). The models can, in principle, accommodate deformation and collision resistance across this boundary. The models do not, however, include features such as a strong, buoyant, underthrust Hikurangi Plateau, which could limit how accurately it will capture collision resistance across such a boundary (e.g., Reyners, 2013). Surface velocity fields for models of Hu et al. (2022) are provided in the original study, and are shown in Supplementary Fig. S3. Euler poles were calculated based on least squares fitting of the velocity grid. Based on these velocity models we make the following observations:

1. In the reference model (MT) of Hu et al. (2022) the Pacific Plate exhibits a NW velocity azimuth at 60 Ma (-48 °, e.g Fig. 2A). This is nearly orthogonal to the calculated azimuth based in the torque due to subduction-related normal forces, based on the same plate reconstruction (-130 °).
2. The inclusion of the IBM has a relatively large effect on the radial component of the rotation, compared to the effect on tangential motion. This observations is based on the model setups that are identical except for the inclusion of the IBM (MN-IBM & MN: shown as yellow and red circles in Figures). These models predict that the IBM induces a 13° (CCW) change in the radial rotation component. Meanwhile the azimuthal change in the tangential velocity is about 9°.
3. The change in the Pacific Plate Euler Pole location, due to the inclusion of the IBM in the numerical models, is along an arc that points almost directly towards Zealandia (as can be seen by comparing the red and yellow markers in Fig 1).
4. When the IBM is not included, the Pacific plate at 47 Ma has negligible radial rotational component ('MN' model, red symbol in Figures). In this model, there is no residual CCW 'signal' which might be identified with the effect of the Zealandia margin, independent from the IBM.

In summary, the models of Hu et al. (2022) suggest that: (1) Pacific Plate motion is sensitive the structure of the subduction boundaries, although other driving forces (along with net slab pull) may be equally important; (2) the inclusion of subduction initiation at the IBM (at 52 Ma) has a relatively large impact on the radial rotation component (at 47 Ma), substantiating the earlier geometric analysis as to high radial torque efficiency of the IBM; (3) The absolute motion changes induced by the IBM, would in turn seem to facilitate Aus-Pac (relative) pivoting, as they move the Pacific Plate Euler Poles towards Zealandia.

Given these conclusions as to the role of the IBM, is there any requirement for collision resistance forces within Zealandia to play a significant additional role? Unfortunately, the models of Hu et al. (2022) do not provide an unambiguous answer to this question. The two models that directly explore the effect of the IBM (MN & MN-IBM), provide an estimate that the IBM produces a 13° CCW radial rotation change. This is about 2/3 of the average CCW radial component throughout 47 - 32 Ma ($\sim$ 18 °) based on the plate reconstruction models. This would apparently leave room for an additional (potentially unmodelled) radial torque component, such as Zealandia collision. Complicating this interpretation, is that fact that the MT model (which also includes the IBM, but no intra-oceanic Kronotsky subduction) predicts a radial rotation component comparable to plate reconstruction models ($\sim$ 18 °). From the numerical models, the effect of Zealandia collision resistance cannot be reliably estimated.

6.2 The role of Zealandia collision

Our geometric analysis tells us about the inherent (geometric) capacity of different plate boundary forces to generate tangential and radial torque components for a given plate. However, it requires additional assumptions in order to compare the torque contributions of different boundaries. For instance, if we assume an equivalent given force density (i.e pull at the IBM and push in the Zealandia collision) we can say that the ratio of the radial torque magnitudes on the Pacific Plate (at 47 Ma) would be about 3:1.

Investigations in numerous settings have concluded that collisional margins may produce force densities equal to or larger than typical subduction related forces (England & Houseman, 1986; Cloetingh & Wortel, 1986; England & Molnar, 2022; Reynolds et al., 2002). Some of these estimates are based on the dynamics of the Himalayan System, in which the GPE component of the collision resistance is large, and potentially inconsistent with the Eocene Zealandia margin. However, significant Eocene shortening and uplift are recorded in Zealandia, such as $\sim$ 12-15 km of motion of the Taranaki fault beginning around 40–43 Ma (Stagpoole & Nicol, 2008), as well as the distributed Eocene deformation of Zealandia that has recently been documented (Sutherland et al., 2020). We also note that the modern day Zealandia Plate boundary (Alpine Fault - Southern Alp System) is thought to transmit margin normal force densities of about 3 TN/m (Reynolds et al., 2002; Sandiford et al., 2004). These magnitudes are similar to the typical estimates of subduction-related forces discussed in Section 1.1.

Hence, the proposition of equivalent force densities between subduction and (e.g. IBM) collisional margins (e.g. Eocence Zealandia) is certainly plausible. To reiterate, based on our analysis for 47 Ma, equal force densities translate to a total radial torque from the Zealandia boundary, that is about 1/3 that of the IBM. If we define first order effects as effects that lie within an order of magnitude of the largest, the speculation of Reyners (2013), appears to be reasonable. The caveat is that this relates only to the radial torque, whereas changes in both radial and tangential motions of the Pacific seem to facilitate the relative Pac-Aus pivoting. In this wider sense, we would suggest Zealandia collision did not have first order effect on Pacific Plate motions.

7 Summary

The overarching problem addressed in the study relates to the pivoting (relative motion) of the Pacific and Australian plates, around an axis lying within or close to Zealandia, during the Eocene. We are motivated by the suggestion that collision resistance (potentially involving the Hikurangi Plateau) had a first order effect on plate motions (Reyners, 2013). In evaluating plate motions in this period, we draw particular attention to the increase in the radial component of the (absolute) Pacific Plate motion at 47 Ma. The pivoting (Pac-Aus) around Zealandia, is partly facilitated by this increased radial component.

The geometric analysis allows us to compare how different plate boundary normal forces contribute to the radial torques that may drive such a change. The geometric analysis highlights the fact that the Eocene IBM trench and the Zealandia margins were both well oriented in terms of partitioning plate boundary normal forces into CCW radial torques on the Pacific Plate. This is particularly so for Zealandia, which has a radial/tangential torque ratio of ~ 1.5. Thus, if Zealandia did have a significant effect on Pac-Aus relative motion, the expression is expected to be largely in the radial component of Pacific Plate motion.

The numerical models support the prediction of the geometric analysis, in terms of the disproportionate effect of the IBM on the radial component of the Pacific motion, but they do not provide a clear conclusion as to the role of Zealandia. This partly due to the nature of that study - models are run both with and without the IBM at 47 Ma, but all models contain the same structure along Zealandia (and it is certainly not guaranteed than this structure accurately represents the nature of that boundary, in particular it neglects the Hikurangi Plateau).

We show that for equivalent force density (i.e force per unit length; pull at the IBM and push at the Zealandia collision) the relative impact of the two boundaries, in terms of radial torque on the Pacific Plate, would be about 3:1. We have briefly addressed some additional constraints on the typical relative magnitude of forces due to collision and subduction. Based on these constraints, Zealandia may have contribute a first order order effect, albeit only on the radial torque.

However, as we have shown, both radial and tangential changes in absolute Pacific Plate motion appear to have facilitated Pac-Aus Euler Poles locating within or close to Zealandia in the middle Eocene. Boundary normal forces along Zealandia have relatively little impact on the Pacific Plate tangential torques, compared to the integrated effect subduction margins. Hence, our analysis suggests that the onset of Pac-Aus pivoting at 47 Ma was a consequence of broader changes in the plate driving/resisting forces, rather than being dominated by force arising from collision resistance across Zealandia.

Viewed in the absolute reference frame (relative to the spin axis), the location of the Pac-Aus Euler Poles have remained quite stable since 47 Ma. In fact, since 47 Ma, they have completed a circuit, first migrating ca. 1500 km eastwards then returning westwards, and currently lie within about 500 kilometers from the 47 Ma locations (i.e. red triangles in Fig. 1, based on the Müller et al. (2016, 2019) reconstructions). In this reference frame, Zealandia has drifted NW away from the location of the Euler Poles. Again, this suggests that the location of the Pac-Aus Euler Poles has been a relatively stable long term feature since ca. 47 Ma., and therefore probably dominated by long wavelength structure of buoyancy in the mantle, to which Pacific Plate subduction provides a major source.

8 Open Research

Plate motion reconstructions used in this study are available from `https://www.earthbyte.org/category/resources/data-models/global-regional-plate-motion-models/`. Geographical figures were made with GPlately (Mather et al., 2023). Velocity grids from numerical models of (Hu et al., 2022) are available at Caltech Data `https://doi.org/10.22002/D1.2150` (see original study).

Acknowledgments

Analysis and figures made use of Python (the 'SciPy' ecosystem). PyGplates and gplately (Mather et al., 2023) software (www.gplates.org) are funded by the AuScope infrastructure-development programme. The work was supported by Australian Research Council grants DP150102887 and DP180102280. The research was facilitated by the flexible and supportive Post Doctoral position provided by Monash University and the aforementioned grants.

References

Anderson, D. L. (2002). Plate tectonics as a far-from-equilibrium self-organized system.

Becker, T. W., & O'Connell, R. J. (2001). Predicting plate velocities with mantle circulation models. *Geochemistry, Geophysics, Geosystems*, *2*(12).

Bercovici, D., Ricard, Y., & Richards, M. A. (2000). The relation between mantle dynamics and plate tectonics: A primer. *Geophysical Monograph-American Geophysical Union*, *121*, 5–46.

Bird, P., Liu, Z., & Rucker, W. K. (2008). Stresses that drive the plates from below: Definitions, computational path, model optimization, and error analysis. *Journal of Geophysical Research: Solid Earth*, *113*(B11).

Cloetingh, S., & Wortel, R. (1986). Stress in the indo-australian plate. *Tectonophysics*, *132*(1-3), 49–67.

Cloetingh, S., Wortel, R., & Vlaar, N. (1989). On the initiation of subduction zones. In *Subduction zones part ii* (pp. 7–25). Springer.

Coblentz, D., van Wijk, J., Richardson, R. M., & Sandiford, M. (2015). The upper mantle geoid: Implications for continental structure and the intraplate stress field. *Geological Society of America Special Papers*, *514*, 197–214.

Colli, L., Stotz, I., Bunge, H.-P., Smethurst, M., Clark, S., Iaffaldano, G., ... Bianchi, M. C. (2014). Rapid south atlantic spreading changes and coeval vertical motion in surrounding continents: Evidence for temporal changes of pressure-driven upper mantle flow. *Tectonics*, *33*(7), 1304–1321.

Conrad, C. P., & Lithgow-Bertelloni, C. (2002). How mantle slabs drive plate tectonics. *Science*, *298*(5591), 207–209.

Eberhart-Phillips, D., Reyners, M., Upton, P., & Gubbins, D. (2018). Insights into the structure and tectonic history of the southern south island, new zealand, from the 3-d distribution of p-and s-wave attenuation. *Geophysical Journal International*, *214*(2), 1481–1505.

Elsasser, W. (1969). Convection and stress propagation in the upper mantle. *The Application of Modern Physics to the Earth and Planetary Interiors, ed. SK Runcorn*, 223–46.

England, P., & Houseman, G. (1986). Finite strain calculations of continental deformation: 2. comparison with the india-asia collision zone. *Journal of Geophysical Research: Solid Earth*, *91*(B3), 3664–3676.

England, P., & Molnar, P. (2022). Changes in plate motions caused by increases in gravitational potential energy of mountain belts. *Geochemistry, Geophysics, Geosystems*, *23*(10), e2022GC010389.

Faccenna, C., Becker, T. W., Lallemand, S., & Steinberger, B. (2012). On the role of slab pull in the cenozoic motion of the pacific plate. *Geophysical Research Letters*, *39*(3).

Forsyth, D., & Uyeda, S. (1975). On the relative importance of the driving forces of plate motion. *Geophysical Journal International*, *43*(1), 163–200.

Gaina, C., Müller, D. R., Royer, J.-Y., Stock, J., Hardebeck, J., & Symonds, P. (1998). The tectonic history of the tasman sea: a puzzle with 13 pieces. *Journal of Geophysical Research: Solid Earth*, *103*(B6), 12413–12433.

Garel, F., Goes, S., Davies, D., Davies, J. H., Kramer, S. C., & Wilson, C. R. (2014). Interaction of subducted slabs with the mantle transition-zone: A regime diagram from 2-d thermo-mechanical models with a mobile trench and an overriding plate. *Geochemistry, Geophysics, Geosystems*, *15*(5), 1739–1765.

Ghosh, A., & Holt, W. E. (2012). Plate motions and stresses from global dynamic models. *Science*, *335*(6070), 838–843.

Gurnis, M., Hall, C., & Lavier, L. (2004). Evolving force balance during incipient subduction. *Geochemistry, Geophysics, Geosystems*, *5*(7).

Hager, B. H., & O'Connell, R. J. (1981). A simple global model of plate dynamics and mantle convection. *Journal of Geophysical Research: Solid Earth*, *86*(B6),

4843–4867.
Holt, A., Becker, T., & Buffett, B. (2015). Trench migration and overriding plate stress in dynamic subduction models. *Geophysical Journal International*, *201*(1), 172–192.
Hu, J., Gurnis, M., Rudi, J., Stadler, G., & Müller, R. D. (2022). Dynamics of the abrupt change in pacific plate motion around 50 million years ago. *Nature Geoscience*, *15*(1), 74–78.
Iaffaldano, G., & Bunge, H.-P. (2015). Rapid plate motion variations through geological time: Observations serving geodynamic interpretation. *Annu. Rev. Earth Planet. Sci*, *43*(1), 571–592.
Iaffaldano, G., & Lambeck, K. (2014). Pacific plate-motion change at the time of the hawaiian-emperor bend constrains the viscosity of earth's asthenosphere. *Geophysical Research Letters*, *41*(10), 3398–3406.
Keller, W. R. (2005). *Cenozoic plate tectonic reconstructions and plate boundary processes in the southwest pacific.* California Institute of Technology.
Lamb, S., Mortimer, N., Smith, E., & Turner, G. (2016). Focusing of relative plate motion at a continental transform fault: Cenozoic dextral displacement¿ 700 km on new zealand's alpine fault, reversing¿ 225 km of late cretaceous sinistral motion. *Geochemistry, Geophysics, Geosystems*, *17*(3), 1197–1213.
Lin, Y.-A., Colli, L., & Wu, J. (2022). Nw pacific-panthalassa intra-oceanic subduction during mesozoic times from mantle convection and geoid models. *Geochemistry, Geophysics, Geosystems*, *23*(11), e2022GC010514.
Mahoney, J., Storey, M., Duncan, R., Spencer, K., & Pringle, M. (1993). Geochemistry and age of the ontong java plateau. *The mesozoic Pacific: Geology, tectonics, and volcanism*, *77*, 233–261.
Mather, B. R., Müller, R. D., Zahirovic, S., Cannon, J., Chin, M., Ilano, L., ... others (2023). Deep time spatio-temporal data analysis using pygplates with plate tectonic tools and gplately. *Geoscience Data Journal*.
McKenzie, D. P. (1969). Speculations on the consequences and causes of plate motions. *Geophysical Journal International*, *18*(1), 1–32.
Moresi, L., & Gurnis, M. (1996). Constraints on the lateral strength of slabs from three-dimensional dynamic flow models. *Earth and Planetary Science Letters*, *138*(1-4), 15–28.
Mortimer, N. (2018). Evidence for a pre-eocene proto-alpine fault through zealandia. *New Zealand Journal of Geology and Geophysics*, *61*(3), 251–259.
Müller, R. D., Seton, M., Zahirovic, S., Williams, S. E., Matthews, K. J., Wright, N. M., ... others (2016). Ocean basin evolution and global-scale plate reorganization events since pangea breakup. *Annual Review of Earth and Planetary Sciences*, *44*(1), 107–138.
Müller, R. D., Zahirovic, S., Williams, S. E., Cannon, J., Seton, M., Bower, D. J., ... others (2019). A global plate model including lithospheric deformation along major rifts and orogens since the triassic. *Tectonics*, *38*(6), 1884–1907.
Reyners, M. (2013). The central role of the hikurangi plateau in the cenozoic tectonics of new zealand and the southwest pacific. *Earth and Planetary Science Letters*, *361*, 460–468.
Reynolds, S. D., Coblentz, D. D., & Hillis, R. R. (2002). Tectonic forces controlling the regional intraplate stress field in continental australia: Results from new finite element modeling. *Journal of Geophysical Research: Solid Earth*, *107*(B7), ETG–1.
Rowley, D. B., & Forte, A. M. (2022). Kinematics of the east pacific rise retrodicted from pacific and farallon/nazca subduction-related torques: Support for significant deep mantle buoyancy controlling epr spreading. *Journal of Geophysical Research: Solid Earth*, *127*(2), e2020JB021638.
Sandiford, M., Coblentz, D., & Schellart, W. P. (2005). Evaluating slab-plate coupling in the indo-australian plate. *Geology*, *33*(2), 113–116.

Sandiford, M., Wallace, M., & Coblentz, D. (2004). Origin of the in situ stress field in south-eastern australia. *Basin Research*, *16*(3), 325–338.
Schellart, W. (2004). Quantifying the net slab pull force as a driving mechanism for plate tectonics. *Geophysical research letters*, *31*(7).
Stadler, G., Gurnis, M., Burstedde, C., Wilcox, L. C., Alisic, L., & Ghattas, O. (2010). The dynamics of plate tectonics and mantle flow: From local to global scales. *science*, *329*(5995), 1033–1038.
Stagpoole, V., & Nicol, A. (2008). Regional structure and kinematic history of a large subduction back thrust: Taranaki fault, new zealand. *Journal of Geophysical Research: Solid Earth*, *113*(B1).
Stotz, I., Iaffaldano, G., & Davies, D. R. (2018). Pressure-driven poiseuille flow: a major component of the torque-balance governing pacific plate motion. *Geophysical Research Letters*, *45*(1), 117–125.
Sutherland, R. (1995). The australia-pacific boundary and cenozoic plate motions in the sw pacific: Some constraints from geosat data. *Tectonics*, *14*(4), 819–831.
Sutherland, R., Collot, J., Bache, F., Henrys, S., Barker, D., Browne, G., … others (2017). Widespread compression associated with eocene tonga-kermadec subduction initiation. *Geology*, *45*(4), 355–358.
Sutherland, R., Dickens, G. R., Blum, P., Agnini, C., Alegret, L., Asatryan, G., … others (2020). Continental-scale geographic change across zealandia during paleogene subduction initiation. *Geology*, *48*(5), 419–424.
Torsvik, T. H., Müller, R. D., Van der Voo, R., Steinberger, B., & Gaina, C. (2008). Global plate motion frames: toward a unified model. *Reviews of geophysics*, *46*(3).
Wessel, P., & Kroenke, L. W. (2008). Pacific absolute plate motion since 145 ma: An assessment of the fixed hot spot hypothesis. *Journal of Geophysical Research: Solid Earth*, *113*(B6).
Whittaker, J., Muller, R., Leitchenkov, G., Stagg, H., Sdrolias, M., Gaina, C., & Goncharov, A. (2007). Major australian-antarctic plate reorganization at hawaiian-emperor bend time. *Science*, *318*(5847), 83–86.

Supporting Information for "A push in the right direction: exploring the role of Zealandia collision in Eocene Pacific-Australia plate motion changes"

Dan Sandiford[1], Peter Betts[1], Joanne Whittaker[2], Louis Moresi[3]

[1]Monash University

[2]University of Tasmania, Institute of Marine and Antarctic Studies

[3]Australian National University

Contents of this file

Figures S1 to S5

References

Doubrovine, P. V., Steinberger, B., & Torsvik, T. H. (2012). Absolute plate motions in a reference frame defined by moving hot spots in the pacific, atlantic, and indian oceans. *Journal of Geophysical Research: Solid Earth*, *117*(B9).

Hu, J., Gurnis, M., Rudi, J., Stadler, G., & Müller, R. D. (2022). Dynamics of the abrupt change in pacific plate motion around 50 million years ago. *Nature Geoscience*, *15*(1), 74–78.

Müller, R. D., Seton, M., Zahirovic, S., Williams, S. E., Matthews, K. J., Wright, N. M., ... others (2016). Ocean basin evolution and global-scale plate reorganization events since pangea breakup. *Annual Review of Earth and Planetary Sciences*, *44*(1), 107–138.

O'Neill, C., Müller, D., & Steinberger, B. (2005). On the uncertainties in hot spot reconstructions and the significance of moving hot spot reference frames. *Geochemistry, Geophysics, Geosystems*, *6*(4).

Reyners, M. (2013). The central role of the hikurangi plateau in the cenozoic tectonics of new zealand and the southwest pacific. *Earth and Planetary Science Letters*, *361*, 460–468.

Wessel, P., & Kroenke, L. W. (2008). Pacific absolute plate motion since 145 ma: An assessment of the fixed hot spot hypothesis. *Journal of Geophysical Research: Solid Earth*, *113*(B6).

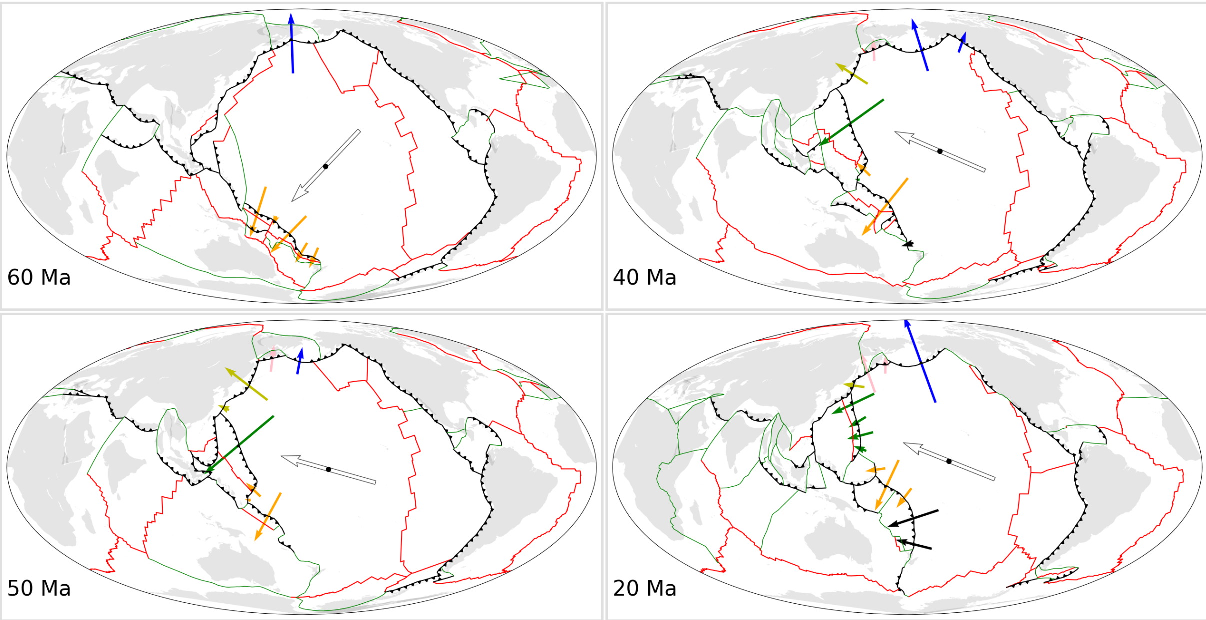

Figure S1. Cenozoic evolution of Pacific subduction margins from Müller et al. (2016). Colored arrows show the net force arising from each boundary segment, with a common scale. The segmentation follows the structure of the underlying dataset. For instance, ar some time periods (e.g. 40 Ma), the IBM (dark green arrows) comprises 1 segment, while at other times it comprises 4 segments (20 Ma). The colors are the same as shown for Fig. 4 in the main manuscript. The white arrow at the plate centroid shows the azimuth of the equivalent force from the tangential torque due to subduction margin forces (not shown to scale across different periods).

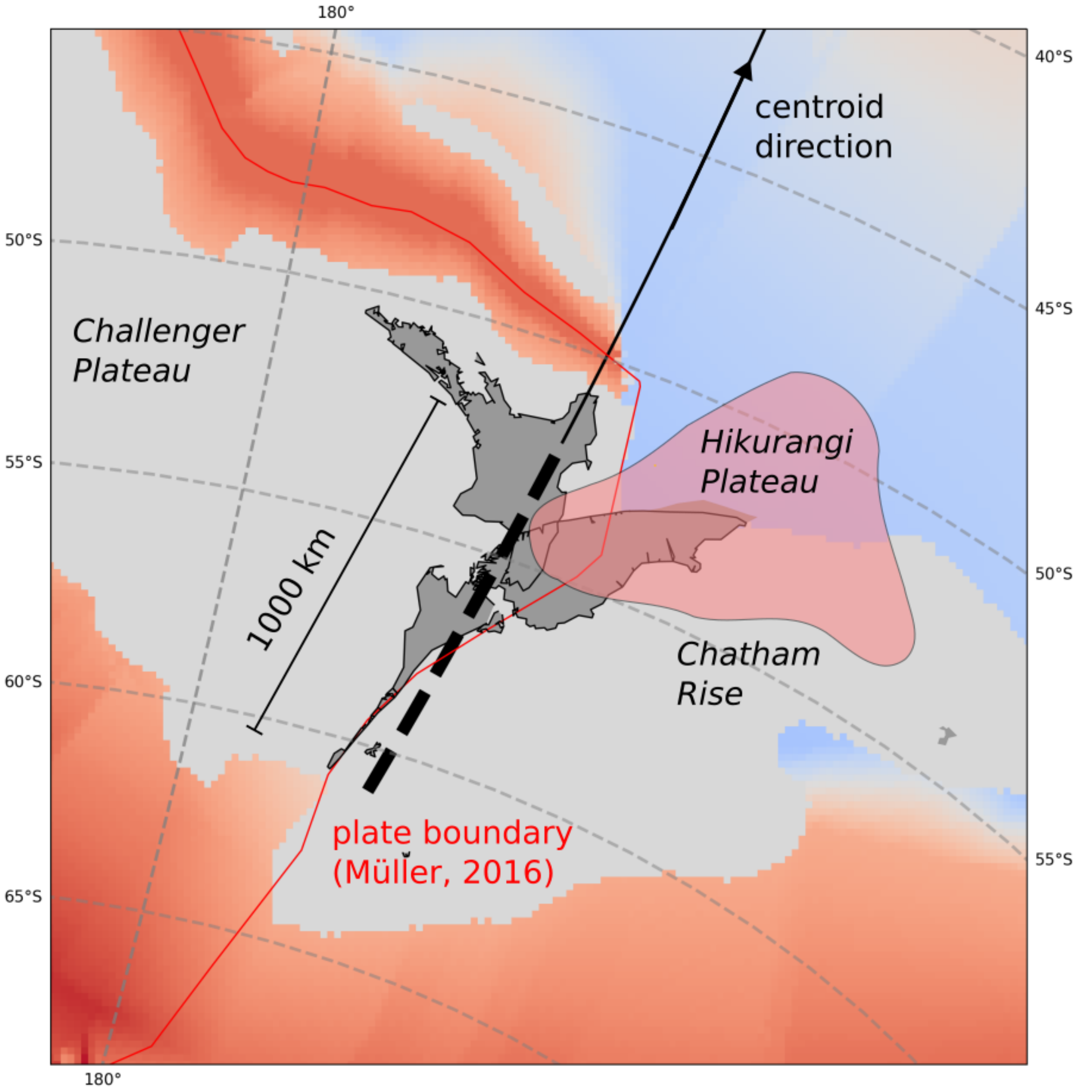

Figure S2. Configuration of Pacific-Australia plate boundary in the Zealandia region at 47 Ma, based on Müller et al. (2016). The colormap shows oceanic lithosphere age, and the grey regions represent continental crust. The pink region shows approximate boundary of the Hikurangi Plateau, based on Reyners (2013). At the time of onset of Pac-Aus pivoting (47 Ma) we assume that the intra-continental part of Zealandia boundary had a length of 1000 km and was parallel with the Pacific Plate centroid direction, as shown by the thick dashed black line.

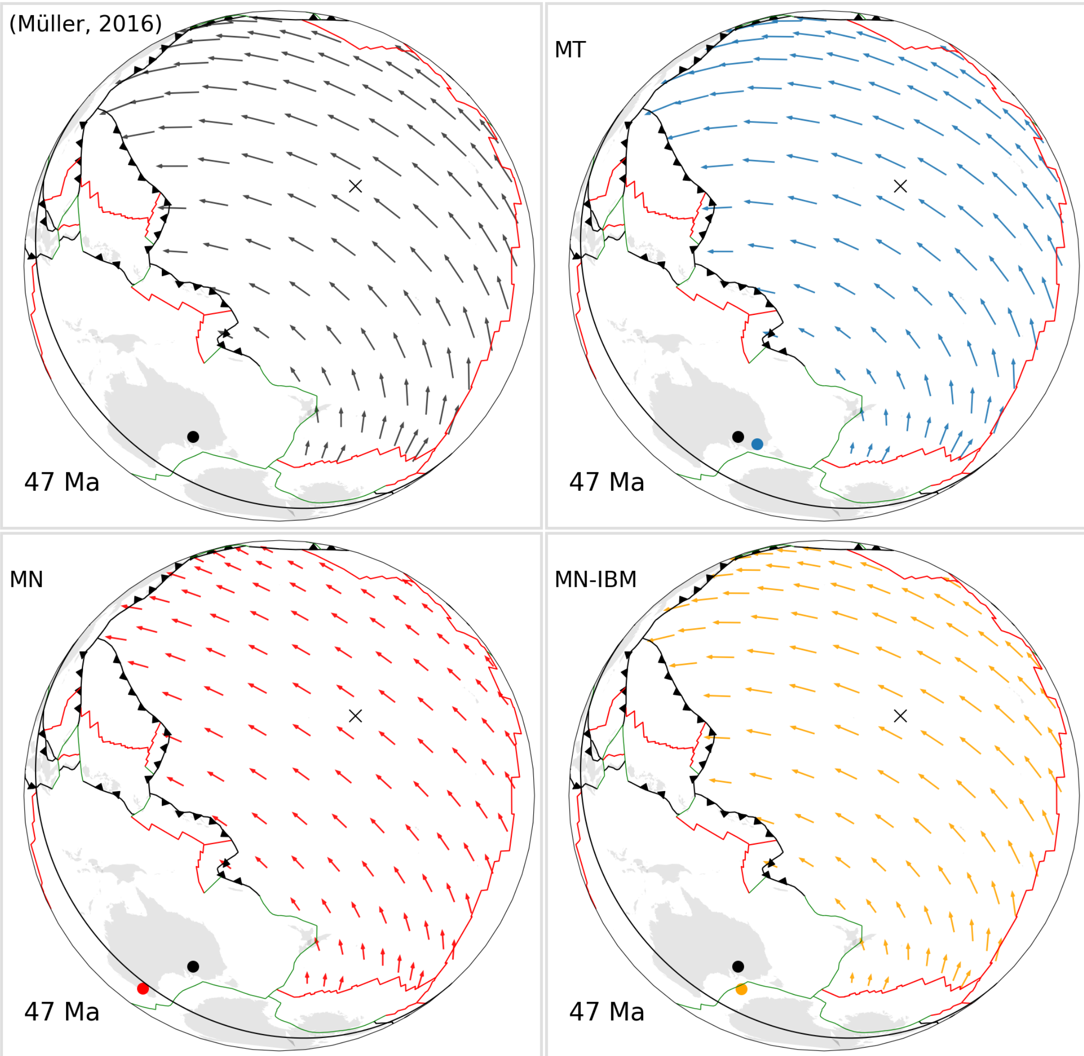

Figure S3. Pacific Plate velocity fields at 47 Ma, in absolute reference frame. Top left shows velocity field from plate reconstruction of Müller et al. (2016). Other panels show velocity fields from global geodynamic models of Hu et al. (2022), labelled according to that study. The Pacific Plate Euler Poles are shown with colored points. The solid black line is the great circle that lies 90° from the Pacific Plate centroid (black cross). Note that in all cases the plate structure shown is from Müller et al. (2016), whereas the "MN" and "MN-IBM" models of Hu et al. (2022) contain modifications to the Pacific Plate boundary. At 47 Ma, these differences are minor however.

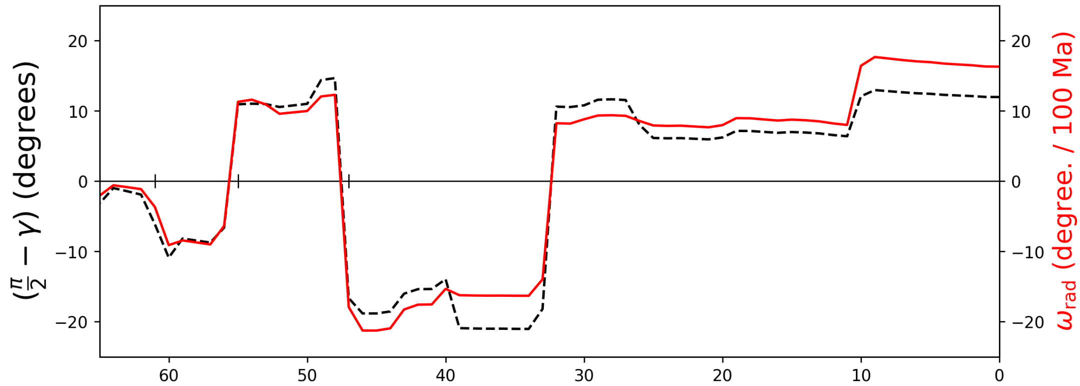

Figure S4. Comparison between the radial component of the Pacific Plate rotation vector ($\vec{\omega}_{\text{rad}} = \vec{\omega} \cdot \hat{r_c}$) shown in red, and the approximation of this value, based on the angle between the Euler Pole and the plate centroid (γ) shown in black.

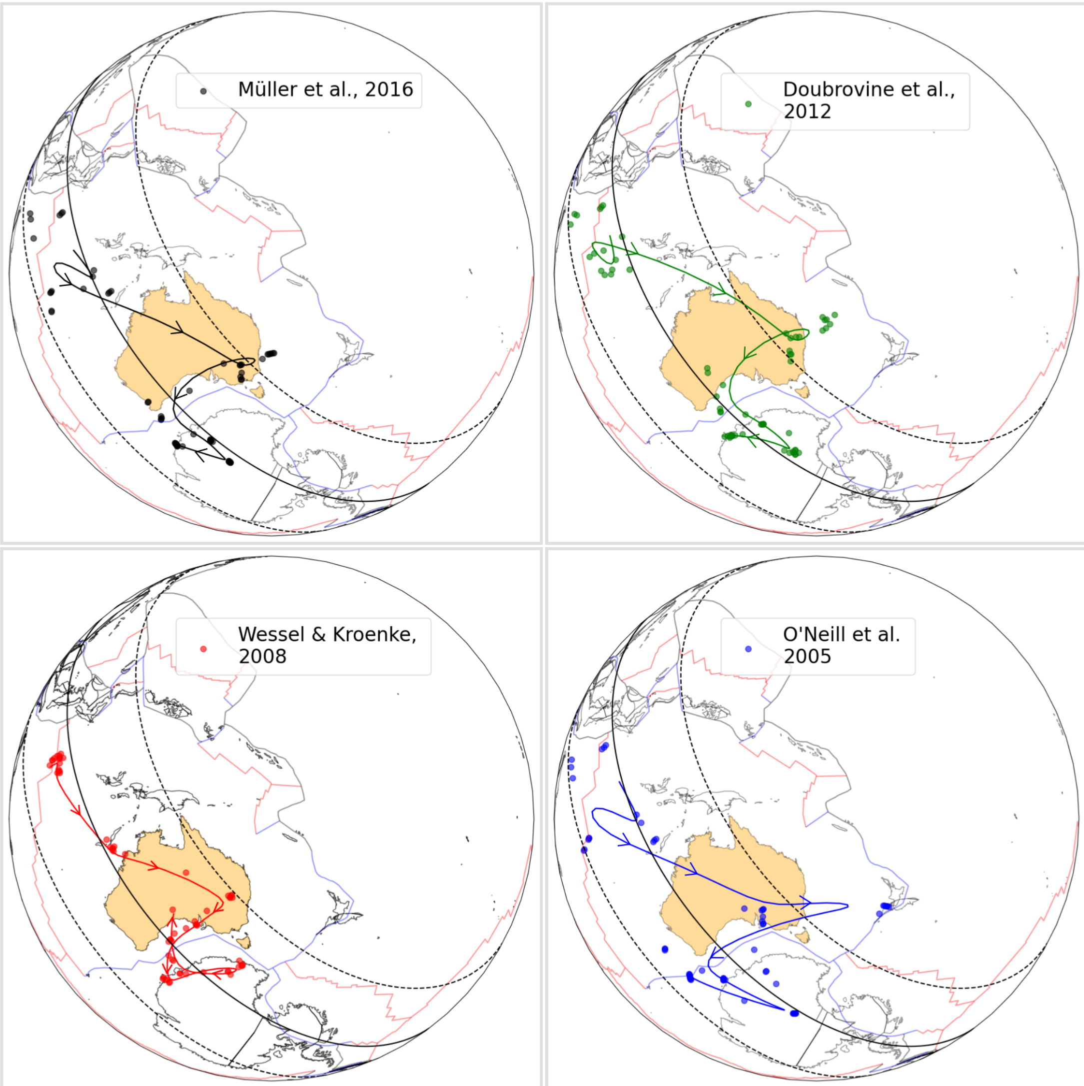

Figure S5. Comparison of Cenozoic Pacific Plate Euler poles in different absolute reference frames. Original studies are Müller et al. (2016); Wessel and Kroenke (2008); Doubrovine et al. (2012); O'Neill et al. (2005). The reference frame from O'Neill et al. (2005) is based in the Tristan Hotspots, as defined in the GPlates *.rot file from Müller et al. (2016). We highlight this particular frame, as it predicts Pacific Plate *absolute* Euler Poles that lie very close to Zealandia. In all cases, the solid line shows the smoothed trajectories of the hotspots, which gives a sense of the overall temporal trends. The model of Wessel and Kroenke (2008) is a fixed Pacific Plate model, and hence in this model the Pacific Plate motion does not depend on a relative motion chain that links the Pacific realm to the Indo-Atlantic. The Euler Poles in the Wessel and Kroenke (2008) reference frame have a small component of random noise added so that separation can be seen between identical poles.